Low CO content hydrogen production from oxidative steam reforming of ethanol over CuO-CeO$_2$ catalysts at low-temperature

Xue Han,   Yunbo Yu,   Hong He*,   Jiaojiao Zhao

Research Center for Eco-Environmental Sciences, Chinese Academy of Sciences, 18 Shuangqing Road, Haidian District, Beijing 100085, China

[Manuscript received February 25, 2013; revised April 18, 2013]

Abstract

CuO-CeO$_2$ catalysts were prepared by a urea precipitation method for the oxidative steam reforming of ethanol at low-temperature. The catalytic performance was evaluated and the catalysts were characterized by inductively coupled plasma atomic emission spectroscopy, X-ray diffraction, temperature-programmed reduction, field emission scanning electron microscopy and thermo-gravimetric analysis. Over CuO-CeO$_2$ catalysts, H$_2$ with low CO content was produced in the whole tested temperature range of 250–450 °C. The non-noble metal catalyst 20CuCe showed higher H$_2$ production rate than 1%Rh/CeO$_2$ catalyst at 300–400 °C and the advantage was more obvious after 20 h testing at 400 °C. These results further confirmed that CuO-CeO$_2$ catalysts may be suitable candidates for low temperature hydrogen production from ethanol.

Key words

CuO-CeO$_2$ catalyst; hydrogen production; oxidative steam reforming; low-temperature

1. Introduction

Ethanol is an important candidate as a chemical carrier of hydrogen, the production of which is useful in a series of fuel cell applications [1–3]. Not only is it less hazardous than methanol, but it can be produced from a variety of biomass sources [4–6]. A typical fuel processor is made up of different processing units such as fuel reformers and CO cleanup reactors. CO cleanup is essential for fuel processor, since the electrodes can only tolerate about 1%–2% CO for phosphoric acid fuel cell (PAFC) and less than 10 ppm for proton exchange membrane fuel cell (PEMFC) [7]. PEMFC and PAFC are classified as low-temperature fuel cells, suitable for automotive applications, operating in the ranges of 80–120 °C and 180–220 °C, respectively. Therefore, if low CO content hydrogen can be produced at low temperatures, this can in turn lower the cost and size of fuel cells by reducing or eliminating the stacks of CO cleanup processing units.

Typical routes for hydrogen production from ethanol are shown in the following equations: steam reforming (SR, Equation 1), partial oxidation (PO, Equation 2), and oxidative steam reforming (OSR, Equation 3).

$$C_2H_5OH + 3H_2O \rightarrow 2CO_2 + 6H_2 \tag{1}$$

$$C_2H_5OH + 1.5O_2 \rightarrow 2CO_2 + 3H_2 \tag{2}$$

$$C_2H_5OH + (3-2x)\,H_2O + xO_2 \rightarrow 2CO_2 + (6-2x)\,H_2$$
$$(0 < x \leqslant 0.5) \tag{3}$$
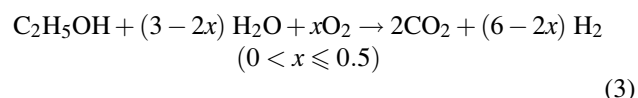
The SR of ethanol provides high hydrogen selectivity, however, it is a highly endothermic reaction, typically operating within the temperature range of 450–700 °C even with the help of catalysts [8,9]. The high reforming temperature also favors the reverse water-gas shift (R-WGS) reaction (CO$_2$+H$_2$→CO+H$_2$O) and thus the generation of CO, the presence of which degrades the performance of Pt electrodes in fuel cell systems [7]. In contrast, the PO of ethanol is an exothermic reaction, the operation temperature of which can be greatly lowered over suitable catalysts. In this case, however, its hydrogen selectivity is decreased [1]. The OSR of ethanol combines both the SR and PO reactions. This means that high hydrogen selectivity can be achieved at low temperatures under OSR conditions with suitable reaction conditions and choice of catalyst.

Ni, Co, Cu and noble metals are common active components which are frequently studied for hydrogen production by steam reforming [10–13]. Although supported noble metal

catalysts, specially Rh, have been demonstrated to exhibit significant activity at low temperatures and high space velocities, the high cost of these metals limits their application [13]. CeO_2 has been extensively utilized as a support for OSR of ethanol mainly due to its remarkable oxygen-storage/release capacity (OSC) and high oxygen mobility, allowing gasification/oxidation of deposited carbon as soon as it forms, and thus improving the catalyst stability [2,9]. Meanwhile, CeO_2 favors ethanol dehydrogenation to acetaldehyde rather than dehydration to ethylene, which is easily polymerizable to coke [14,15]. Furthermore, CuO-CeO_2 catalysts have good activity for the oxidation of CO in a hydrogen-rich stream [16] and their catalytic performance for hydrogen production from SR of ethanol has been reported [13]. Inspired by all of the above, we employed CuO-CeO_2 mixed oxide as a catalyst for OSR reaction for the first time.

It has been extensively reported that CuO-CeO_2 materials can be prepared by hydrothermal treatments [17,18], a hard template method [13] and combustion method [19–21]. However, the former two methods are complicated and the combustion method tends to lead to low surface area. In this work, CuO-CeO_2 catalysts with varying $Cu/(Cu+Ce)$ mole ratio were prepared by urea co-precipitation, which is a homogeneous precipitation method, characterized by a highly uniform increase in pH value of metal salts solution. It is a convenient method for catalyst preparation that can produce highly dispersed mixed metal oxides [22]. The H_2 yield rate and product distribution of CuO-CeO_2 catalysts under OSR conditions with high space velocity were tested and compared with $1\%Rh/CeO_2$ catalyst.

2. Experimental

2.1. Catalyst preparation

CeO_2 and CuO-CeO_2 mixed oxides catalysts with nominal CuO contents of 10, 20, 30 and 40 mol% were synthesized by a urea precipitation method. Appropriate amounts of copper (II) nitrate hexahydrate ($Cu(NO_3)_2 \cdot 3H_2O$, 99%) and cerium (III) nitrate hexahydrate ($Ce(NO_3)_3 \cdot 6H_2O$, 99%) were dissolved in water together with urea, and the metal ion concentration ($Cu+Ce$) was fixed at 0.5 mol/L. After stirring for 24 h at 90 °C, the precipitate was dried at 100 °C for 12 h, and then thermally treated in a furnace at 500 °C for 5 h in air. CuO-CeO_2 mixed oxides catalysts were expressed as mCuCe, where m is the nominal CuO content. For comparison, a CeO_2-supported Rh catalyst was also prepared by an impregnation method, followed by drying at 100 °C for 12 h and calcination at 500 °C for 3 h in air. Rhodium loading was fixed at 1 wt% and the precursor was $RhCl_3 \cdot 3H_2O$. This CeO_2-supported Rh catalyst was expressed as $1\%Rh/Ce$.

2.2. Catalyst characterization

The BET surface area, average pore diameter and total pore volume of catalysts were determined on Autosorb iQ-1MP automatic equipment by physical adsorption measurement with N_2 at –196 °C. Prior to N_2 physical sorption, the samples were degassed.

The chemical composition of the catalyst was determined by inductively coupled plasma atomic emission spectroscopy (ICP-AES) using an OPTIMA 2000DV spectrometer.

X-ray powder diffraction (XRD) patterns were measured using a PANalytical X'Pert Pro diffractometer with Cu K_α ($\lambda = 0.15406$ nm) radiation. The data were collected for 2θ from 10° to 90° at 6 °/min with a step size of 0.026°.

The surface morphologies of fresh and used catalysts were studied by SU-8020 field emission scanning electron microscopy (FE-SEM). Powder samples were mounted directly on aluminum sample holders and placed in SEM chamber without gold sputter coating.

Hydrogen temperature-programmed reduction (H_2-TPR) measurements were carried out in a conventional set-up equipped with a thermal conductivity detector (TCD). Samples (200 mg) were heated from room temperature to 800 °C in a reducing gas mixture (10 vol% H_2/He, 50 mL·min^{-1}) at a ramp rate of 10 °C·min^{-1}.

The carbon deposition rates over catalysts during OSR reaction were measured by thermo-gravimetric analysis (TGA, STARe system METTLER TOLEDO) method. The aged catalyst were heated in pure O_2 (50 mL·min^{-1}) from 30 to 900 °C at a heating rate of 20 °C·min^{-1}. Simultaneously, the weight change of the employed catalyst was measured with time on-stream.

2.3. Catalytic test

The OSR reaction of ethanol was carried out in a continuous-flow fixed-bed microreactor made of a quartz tube of 6 mm in inner diameter with 100 ± 2 mg catalyst (40–60 mesh, diluted with 300 mg SiO_2). A mixture of ethanol and water was supplied by a syringe pump at a rate of 0.06 mL·min^{-1}. After being sufficiently vaporized by passing through a preheating zone at 150 °C, this mixture was continuously fed into the reactor together with N_2 carrier and O_2 ($EtOH : H_2O : O_2 = 1 : 3 : 0.5$), with a mixed gas flow rate of 350 mL·min^{-1}. The reaction temperature (measured with a thermocouple located in the middle of the catalyst bed) was increased in 25 °C increments from 250 to 450 °C, and each temperature point was maintained for at least 1 h. The liquid products were removed by condensation and then the effluent gases were analyzed on-line at each temperature point using a gas chromatograph (Shimadzu, GC-2014C) equipped with two TCDs and one FID. The TCDs detection limits of N_2, H_2, CO, CO_2 and CH_4 products were 200 ppm.

Since this work was carried out at on-board conditions, a room temperature normal flow rate (F_x) that takes the volume change into account was considered to calculate H_2 yield rate and product distribution:

$$F_x = \frac{[X] \times F_{N_2}}{[N_2]} \qquad (4)$$

where, F_{N_2} is the N_2 flow rate at room temperature, $[N_2]$ is

the concentration of N_2 (%), and [X] is the concentration of X (%). H_2 formation rate was calculated according to Equation (5) where F_{H_2} represents the normal flow rate of H_2.

$$R_{H_2} = \frac{F_{H_2}}{\text{Weight of catalyst}} \qquad (5)$$

The distribution of products was calculated according to the following equation:

$$D_x = \frac{F_x}{F_{H_2} + F_{CO} + F_{CH_4} + F_{CO_2}} \qquad (6)$$

CO gas water shift reaction was carried out in the same microreactor with feed gas compositions of 1% CO and 3% water (N_2 balance) from 250 to 450 °C. The mixed gas flow rate was kept at 350 mL·min^{-1}. In this study, the catalyst stability test was also carried out at 400 °C for 20 h under the same OSR reaction conditions.

3. Results and discussion

3.1. Characterization of catalysts

The results of BET surface area, elemental analysis (analyzed by ICP-AES) and average crystallite size (analyzed by XRD) of CuO-CeO_2 catalysts (mCuCe, m stands for the mol% of Cu to Cu+Ce) are summarized in Table 1. The surface area of ceria decreased from 59 to 44 m^2·g^{-1} after loading with 1 wt% Rh. The BET results also showed that mCuCe catalysts had much higher surface area compared with pure CeO_2 and 1%Rh/CeO_2 (1%Rh/Ce). Among mCuCe mixed oxides, 20CuCe catalyst had the largest surface area (96 m^2·g^{-1}). It has been reported that high surface area corresponds to high dispersal of CuO in/on CeO_2; however, if the copper content of the composite was much higher than the dispersion capacity of CeO_2, a dramatic decrease of the catalytic activity would occur [13,18]. According to the results of ICP-AES, the actual Cu concentrations of mCuCe catalysts by molar percentage were lower than the nominal contents, being 5.6% for 10CuCe, 12% for 20CuCe, 23% for 30CuCe and 35% for 40CuCe, respectively; while Rh concentration of 1%Rh/Ce catalyst was 1.0 wt%. It was clear that the Cu contents in mCuCe catalysts were much less than the nominal contents. To explain this phenomenon, 10CuCe and 20CuCe samples were also prepared using NaOH as a precipitant. The Cu concentration in this case was 9.8% for 10CuCe and 19.2% for 20CuCe. The discrepancy can be explained by the fact that the basicity of urea is much weaker than NaOH, which results in incomplete precipitation. The average crystallite sizes of the catalysts were calculated by applying the Scherer equation to the characteristic (111) peak of CeO_2 from XRD results. Pure CeO_2 had a crystallite size of 17.8 nm, which increased to 20.6 nm after loading with Rh, but it decreased considerably to 11.9–14.4 nm in the case of mCuCe catalysts (Cu concentration = 5.6–35 mol%). These crystallite sizes were in quantitative agreement with BET surface area results.

Figure 1 presents the XRD patterns of fresh mCuCe, pure CeO_2 and 1%Rh/Ce catalysts. It can be clearly seen

that a fluorite-type structure of ceria with lattice constant $a = 5.411$ Å was present in all the samples. For low-Cu-containing catalysts, such as 10CuCe and 20CuCe, no reflections indexed to copper oxide phases were found; while for 30CuCe and 40CuCe, the monoclinic phase of CuO with lattice constants $a = 4.685$ Å, $b = 3.432$ Å and $c = 5.132$ Å coexisted with ceria. The weak or absent CuO phase peaks in XRD patterns may be attributed to the fine dispersion of CuO particles on the surface of ceria so that the peaks were beyond the detection limit of XRD, or the formation of an interfacial solid solution [20,23]. It was reported that if there is any substitution of Cu^{2+} ion in Ce^{4+} site, the lattice parameter should decrease, as the ionic radius of Cu^{2+} (0.76 Å) is smaller than that of Ce^{4+} (0.92 Å) and Ce^{3+} (1.03 Å), thus shifting the diffraction peaks toward higher 2 theta (it is the inverse if Ce^{4+} is replaced by Ce^{3+}) [19,24]. However, going from pure CeO_2 to 1%Rh/Ce or mCuCe materials, the shift of XRD peaks as shown in Figure 1 was within 0.02° and the change of lattice parameter a was within 0.005 Å, calculated from XRD analysis. Considering this limited information, it is probable that a small portion of Cu formed a Ce-Cu solid solution and the rest existed as CuO. Therefore, the weak or absent CuO diffraction peaks of mCuCe catalysts can be mainly ascribed to the well-dispersed small CuO crystallites on the surface of CeO_2.

Table 1. Physical properties of different samples

Catalysts	Surface area (m^2·g^{-1})	Average pore diameter (nm)	Total pore volume (cm^3·g^{-1})	Cu/ (Cu+Ce) (mol%)	Average crystallite size (nm)
CeO$_2$	59	5.4	0.06	–	17.8
1%Rh/Ce	44	6.1	0.05	–	20.6
10CuCe	85	4.9	0.10	5.6	13.6
20CuCe	96	5.4	0.13	12	11.9
30CuCe	84	3.4	0.07	23	13.0
40CuCe	75	4.8	0.09	35	14.4
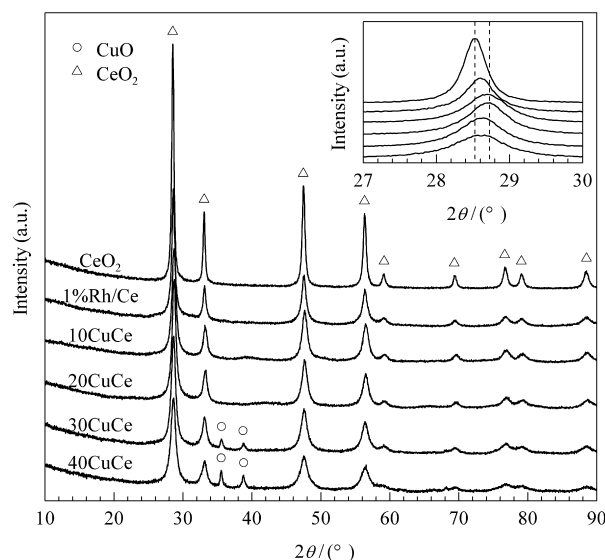
Figure 1. XRD patterns of CeO$_2$, 1%Rh/Ce and mCuCe samples

Figure 2 shows SEM images of the catalysts. CeO$_2$ and 1%Rh/Ce catalysts exhibited a similar cracked triangular-prism-like surface morphology. For 10CuCe, 20CuCe and 30CuCe catalysts, the SEM images seemed like rod; while it became very irregular for 40CuCe. It is worth to be noted that 20CuCe catalyst had much smaller particular size than the other samples. XRD results (Table 1) also indicate that 20CuCe catalyst had the smallest average crystalline sizes of 11.9 nm. The particular size seemed to be bigger than crystalline size, because the former was combined by the letter and SEM offered the real micrograph like a camera; while average crystalline size from XRD were estimated from predominant planes by Scherer equation.
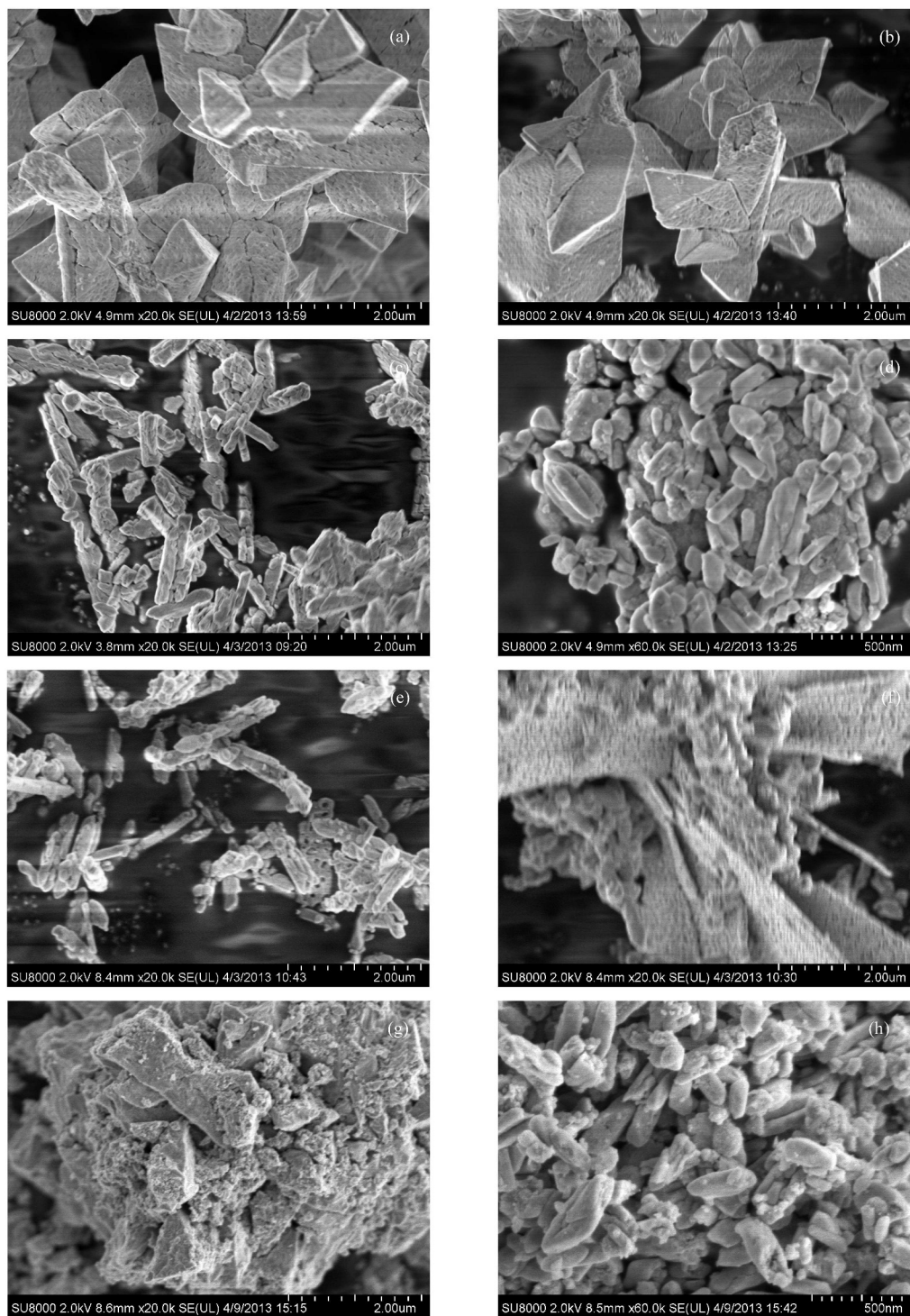
Figure 2. SEM micrographs of CeO$_2$ (a), 1%Rh/Ce (b), 10CuCe (c), 20CuCe (d), 30CuCe (e), 40CuCe (f), 1%Rh/Ce-used (g) and 20CuCe-used (h)

Figure 3 shows the TPR profiles of mCuCe catalysts, CeO$_2$ and 1%Rh/Ce were also presented for comparison. The pure CeO$_2$ had two reduction peaks at about 460 and 820 °C (the high temperature reduction peak is not shown in this figure), ascribed to the reduction of surface cerium and bulk cerium, respectively [18,25,26]. After loading with 1 wt% Rh, the reduction temperatures moved to 105 and 310 °C, respectively. mCuCe catalysts mainly showed two reduction peaks at 158–169 °C and 185–190 °C, respectively. It is interesting to note that the temperature interval and overall shape of the recorded TPR curves of mCuCe catalysts did not differ much when Cu content was increased. As reported by Djinovic et al. [13], this feature reveals the presence of finely dispersed CuO on CeO$_2$, with strong electronic interactions between both metal oxide phases in all tested samples. The XRD results had already confirmed the presence of CuO phase when Cu content was >20 mol%, and the formation of Ce-Cu solid solution when Cu was <15 mol%. All of the above mean that CuO and Ce-Cu solid solution coexisted in mCuCe catalysts. Cu replaced a portion of Ce in the pure ceria supports. Therefore, mCuCe catalysts can be taken as Ce-Cu solid solution-supported CuO. Over each sample containing copper, the low temperature reduction peak can be ascribed to the reduction of finely dispersed surface copper species strongly interacting with the support [18]. As a result, the reduction of surface CuO was affected by the support, while not having a close relationship with Cu content and surface area. The higher temperature peak can be assigned to the reduction of bulk CuO interacting with the support [21]. In addition, with increasing levels of Cu doping, the intensities of reduction peaks at high temperatures increased greatly. These data indicate that CuO was present in all the mCuCe samples and a portion of Cu entered into the ceria lattice and formed a Ce-Cu solid solution.
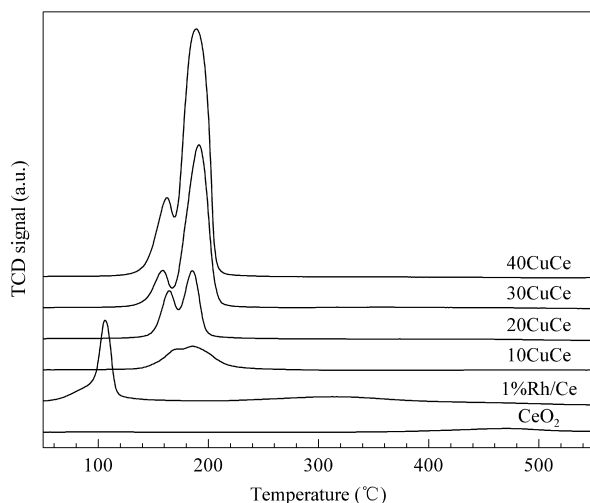
Figure 3. H$_2$-TPR profiles of CeO$_2$, 1%Rh/Ce and mCuCe samples

3.2. Catalytic performance

Figure 4 shows the catalytic performance of 1%Rh/Ce catalyst and mCuCe catalysts. It can be seen from Figure 4(a) that 20CuCe catalyst had the highest hydrogen formation rate among various CuCe catalysts, being even higher than that of 1%Rh/Ce in the temperature range of 300–400 °C. The hydrogen formation rate of mCuCe catalysts increased with Cu loading; however, when the nominal Cu content was above 20 mol%, the hydrogen yield rate decreased greatly. Taking 450 °C as an example, the hydrogen formation rate of mCuCe catalysts normalized by surface area decreased in the order of 20CuCe (0.102 NL·h^{-1}·m^{-2})>10CuCe (0.062 NL·h^{-1}·m^{-2})>30CuCe (0.049 NL·h^{-1}·m^{-2})>40CuCe (0.045 NL·h^{-1}·m^{-2}). Combined with the catalyst characterization results, this indicates that increasing Cu content can greatly increase the hydrogen formation rate per unit surface area, when nominal Cu content was lower than 20 mol%. However, excess CuO no longer maintained a fine dispersion in Ce-Cu solid solution, resulting in a decrease of surface area and more dramatic decrease of catalytic activity. This implies that a moderate CuO content and high surface area tended to guarantee the good catalytic performance in OSR reaction. The Cu content of the most active mCuCe catalyst (20CuCe) was 12 mol%. It was also reported by Djinovic et al. and Delimaris et al. [13,20] that catalytic activity was obtained at Cu/(Cu+Ce) = 10%–15% for VOC oxidation and steam reforming of ethanol, respectively.

At 450 °C, 1%Rh/Ce catalyst produced the highest H$_2$ formation rate; however, H$_2$ distribution (D_{H_2}) in its products (Figure 4b) was lower than that of mCuCe catalysts at the same temperature. In addition, CO and CH$_4$ production over 1%Rh/Ce catalyst were more than 5% over the whole temperature range, which lowered H$_2$ percentage. Over mCuCe catalysts, it is worth noting that CO and CH$_4$ were undetected (less than 200 ppm). This means that, in the product mixed gas flow, there was only H$_2$, CO$_2$ and inert gas such as N$_2$ after removal of residual ethanol and liquid products by condensation. In other words, the hydrogen produced over mCuCe catalysts was pure enough for direct application to fuel cells, and needed no additional CO cleanup reactor. Furthermore, 20CuCe had a higher hydrogen yield rate than ceria-supported noble metal catalyst, so it can be used to lower the catalyst cost.

The water gas shift (WGS, CO+H$_2$O → CO$_2$+H$_2$) reaction is a very important intermediate reaction for the OSR of ethanol, which leads to the removing of CO and H$_2$ production. To understand the reaction role, 1% CO and 3% water were fed through 20CuCe and 1%Rh/Ce catalysts in OSR reaction under the same space velocity. As shown in Figure 5, CO concentration over both catalysts decreased with temperature. In the temperature range of 250–425 °C, CO concentration of 20CuCe was higher than that of 1%Rh/Ce. A high WGS activity contributes to lower CO content. Considering that CO production was undetected over 20CuCe catalyst, there might be another CO removing reaction, such as CO oxidation (CO+O$_2$→CO$_2$). When 1.5% CO and 1.7% O$_2$ were fed through 20CuCe catalyst in OSR reaction under the same space velocity, no CO was detected in the temperature range of 250–450 °C (data not shown).
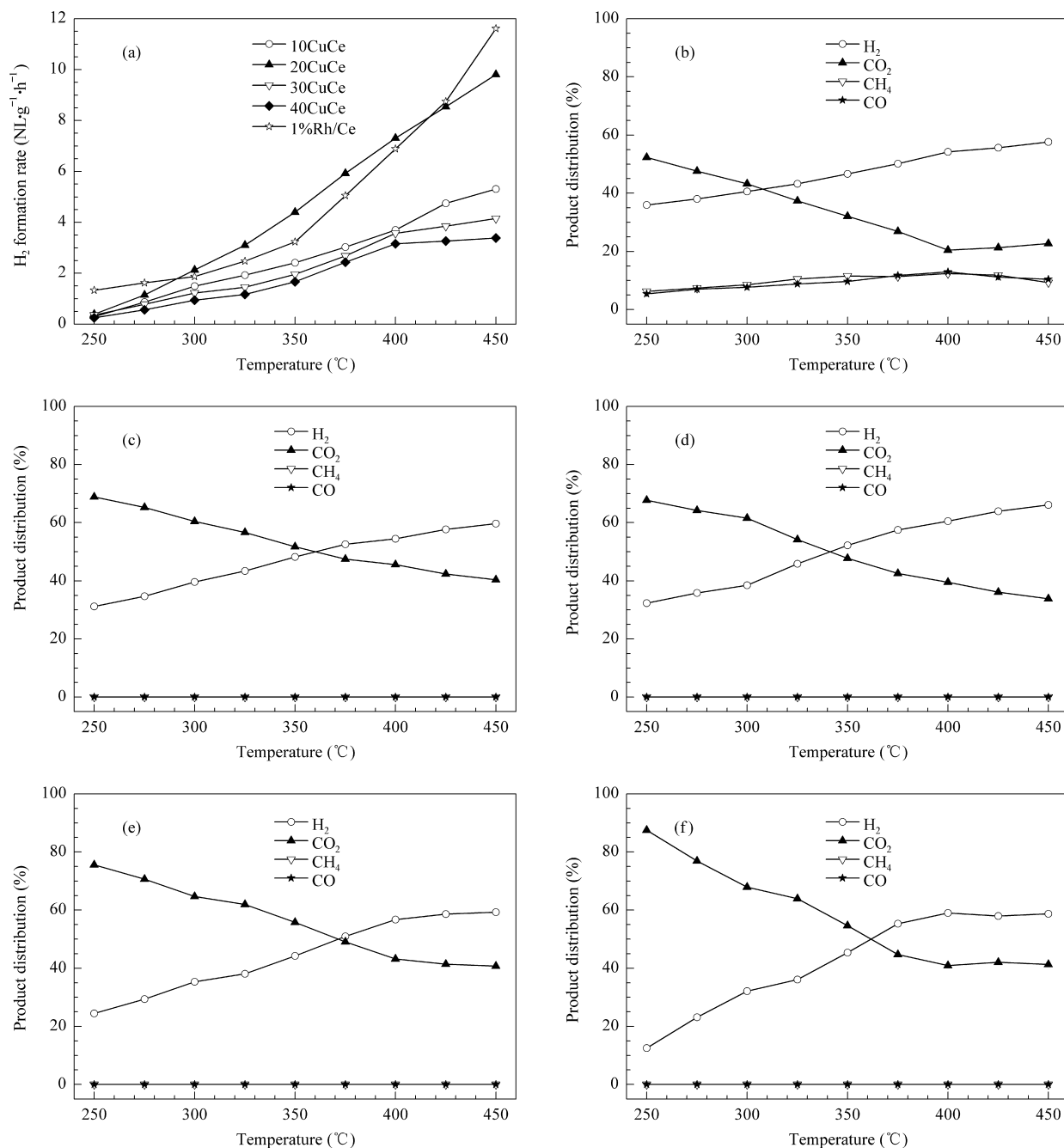
Figure 4. Catalytic performances of 1%Rh/Ce and mCuCe catalysts from 250 to 450 °C. (a) H_2 formation rate on different catalysts; production distribution on (b) 1%Rh/Ce, (c) 10CuCe, (d) 20CuCe, (e) 30CuCe and (f) 40CuCe

3.3. Stability

The stability of 1%Rh/Ce and 20CuCe was tested for 20 h at 400 °C under the same OSR reaction conditions. Figure 2(g) and 2(h) show SEM micrographs of the used 1%Rh/Ce and used 20CuCe catalysts. An obvious difference was found between the fresh (Figure 2b) and used 1%Rh/Ce (Figure 2g) catalysts, which can be explained by the formation of a lot of analogous carbon compounds on the catalyst surface during the OSR reaction process [27]. However, the SEM micrographs did not show a big difference between the

fresh (Figure 2d) and used 20CuCe (Figure 2h) catalysts.

Figure 6 shows TGA results of the used 1%Rh/Ce and 20CuCe catalysts. The mass loss at around 130 °C was assigned to the desorption of physically and chemically adsorbed H_2O [28]. The used 1%Rh/Ce and 20CuCe catalysts had obvious mass loss at 245 °C and 280 °C, respectively, which is corresponding to the burning of deposited coke in oxygen.

Table 2 compares the ethanol conversion and product yields of the fresh and used catalysts, the effluent gases

were analyzed on-line without condensation (carbon mass balance = 100±5%). After 20 h using, both of 1%Rh/Ce and 20CuCe catalysts showed obvious deactivation. As compared with 1%Rh/Ce, 20CuCe catalyst yielded more CH_3COCH_3, which is a main precursor for coke deposition. It explained why mass loss of used 20CuCe was the more than that of used 1%Rh/Ce. However, it is noticed that H_2 yield of used 20CuCe catalyst was much higher than that of 1%Rh/Ce, in other words, 20CuCe had better H_2 production stability. It may be the reason that the surface structure of 1%Rh/Ce was greatly changed after carbon deposition during aging and its stability was affected; while the deposited coke had less effect on the surface structure of the used 20CuCe catalyst and its stability.
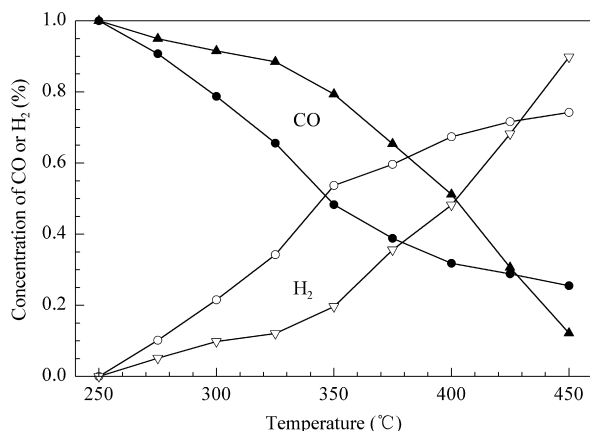
Figure 5. CO concentrations over 20CuCe (●) and 1%Rh/Ce (▲) catalysts and H_2 over 20CuCe (○) and 1%Rh/Ce (▽) catalysts for WGS reaction from 250 °C to 450 °C
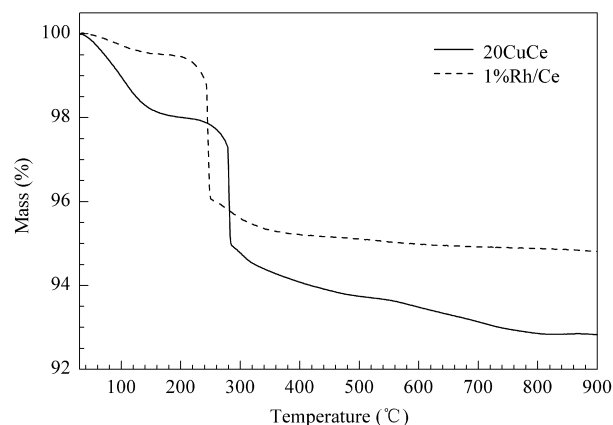
Figure 6. TGA curves of used 1%Rh/Ce and 20CuCe catalysts

Table 2. Ethanol conversion and product yields on different catalysts

Catalysts	EtOH conversion (%)	Product yield (100 mol/mol$_{EtOH}$)					
		H_2	CO_2	CH_4	CO	CH_3CHO	CH_3COCH_3
20CuCe	69.3	144	96.2	0	0	9.1	7.6
20CuCe-used	36.4	76.4	53.4	0	0	4.6	2.6
1%Rh/Ce	80.9	132	50.2	31.2	29.6	17.7	6.4
1%Rh/Ce-used	48.0	20.2	34.2	19.2	16.4	10.4	1.2

4. Conclusions

*m*CuCe catalysts existed as Cu-Ce solid solution-supported CuO. Under the OSR reaction conditions, low CO content (undetectable) H_2 was produced over these catalysts. The outlet gas flow contained only H_2, CO_2 and inert gas, hence downstream CO clean-up reactors can be reduced or eliminated in the fuel cell system. Furthermore, the H_2 production rate over 20CuCe catalyst was higher than that over ceria-supported Rh catalyst in the temperature range of 300–400 °C and after using 20 h this advantage was more obvious, which makes it a good catalyst candidate for H_2 production from ethanol. Increasing CuO content helped enhance the catalytic activity, but if it exceeded the dispersion capacity of Ce-Cu solid solution support, the catalytic activity decreased dramatically.

Acknowledgements

References

[1] Mattos L V, Jacobs G, Davis B H, Noronha F B. *Chem Rev*, 2012, 112(7): 4094

[2] Liu Q H, Liu Z L, Zhou X H, Li C J, Ding J. *J Rare Earths*, 2011, 29(9): 872

[3] Foad M, Majid T. *J Nat Gas Chem*, 2012, 21(5): 526

[4] Ni M, Leung D Y C, Leung M K H. *Int J Hydrog Energy*, 2007, 32(15): 3238

[5] Han X, Yu Y B, He H, Zhao J J, Wang Y F. *J Power Sources*, 2013, 238: 57

[6] Wang B W, Lu Y J, Zhang X, Hu S H. *J Nat Gas Chem*, 2011, 20(2): 151

[7] Chen L W, Choong C K S, Zhong Z Y, Huang L, Ang T P, Hong L, Lin J Y. *J Catal*, 2010, 276(2): 197

[8] Chen H Q, Yu H, Peng F, Wang H J, Yang J, Pan M Q. *J Catal*, 2010, 269(2): 281

[9] Song H, Ozkan U S. *J Catal*, 2009, 261(1): 66

[10] Vaidya P D, Rodrigues A E. *Chem Eng J*, 2006, 117(1): 39

[11] Haryanto A, Fernando S, Murali N, Adhikari S. *Energy Fuels*, 2005, 19(5): 2098

[12] Pang X J, Chen Y Z, Dai R Q, Cui P. *Chin J Catal (Cuihua Xuebao)*, 2012, 33(2): 281

[13] Djinovic P, Batista J, Cehic B, Pintar A. *J Phys Chem A*, 2010, 114(11): 3939

[14] Idriss H. *Platin Met Rev*, 2004, 48(3): 105

[15] Bion N, Duprez D, Epron F. *ChemSusChem*, 2012, 5(1): 76

[16] Hornés A, Hungría A B, Bera P, López Cámara A, Fernández-García M, Martínez-Arias A, Barrio L, Estrella M, Zhou G, Fonseca J J, Hanson J C, Rodriguez J A. *J Am Chem Soc*, 2010, 132(1): 34

[17] Qin J W, Lu J F, Cao M H, Hu C W. *Nanoscale*, 2010, 2(12): 2739

[18] Mai H L, Zhang D S, Shi L Y, Yan T T, Li H R. *Appl Surf Sci*, 2011, 257(17): 7551

[19] Bera P, Priolkar K R, Sarode P R, Hegde M S, Emura S, Kumashiro R, Lalla N P. *Chem Mater*, 2002, 14(8): 3591

[20] Delimaris D, Ioannides T. *Appl Catal B*, 2009, 89(1-2): 295

[21] Shan W J, Shen W J, Li C. *Chem Mater*, 2003, 15(25): 4761

[22] Shan W P, Liu F D, He H, Shi X Y, Zhang C B. *Chem Commun*, 2011, 47(28): 8046

[23] Jia A P, Hu G S, Meng L, Xie Y L, Lu J Q, Luo M F. *J Catal*, 2012, 289: 199

[24] Shan W J, Feng Z C, Li Z L, Jing Z, Shen W J, Can L. *J Catal*, 2004, 228(1): 206

[25] Zhang B C, Cai W J, Li Y, Xu Y D, Shen W J. *Int J Hydrog Energy*, 2008, 33(16): 4377

[26] Kugai J, Velu S, Song C S. *Catal Lett*, 2005, 101(3-4): 255

[27] Wang Y H, Zhang J C. *Fuel*, 2005, 84(14-15): 1926

[28] Hu J Y, Liu X Y, Wang B, Pei Y, Qiao M H, Fan K N. *Chin J Catal (Cuihua Xuebao)*, 2012, 33(8): 1266